THE JOURNAL OF BIOLOGICAL CHEMISTRY VOL. 286, NO. 40, pp. 34486–34496, October 7, 2011

Elevated Calcium Acutely Regulates Dynamic Interactions of NHERF2 and NHE3 Proteins in Opossum Kidney (OK) Cell Microvilli*

Received for publication, February 11, 2011, and in revised form, July 21, 2011 Published, JBC Papers in Press, July 28, 2011, DOI 10.1074/jbc.M111.230219

Xinjun Zhu[‡§1,2], Boyoung Cha[‡1], Nicholas C. Zachos[‡], Rafiquel Sarker[‡], Molee Chakraborty[‡], Tian-e Chen[‡], Olga Kovbasnjuk[‡], and Mark Donowitz[‡¶3]

From the Departments of [‡]Medicine and [¶]Physiology, Division of Gastroenterology, The Johns Hopkins University School of Medicine, Baltimore, Maryland 21205 and the [§]Gastrointestinal Division, Albany Medical College, Albany, New York 12008

Background: Na/H exchanger 3 is fixed to the BB cytoskeleton but is regulated by changes in trafficking.
Results: Elevated Ca^{2+} rapidly decreases BB NHE3 amount/activity and transiently decreases NHE3 association with NHERF2 and increases NHE3 BB mobility.
Conclusion: There is coordinated regulation of trafficking and NHE3 BB cytoskeletal association.
Significance: A newly recognized aspect of signal transduction in epithelial cells is dynamic/transient changes in BB transporter-cytoskeleton association.

The brush border (BB) Na^+/H^+ exchanger NHE3 is rapidly activated or inhibited by changes in trafficking, which mimics renal and intestinal physiology. However, there is a paradox in that NHE3 has limited mobility in the BB due to its binding to the multi-PDZ domain containing the NHERF family. To allow increased endocytosis, as occurs with elevated intracellular Ca^{2+}, we hypothesized that NHE3 had to be, at least transiently, released from the BB cytoskeleton. Because NHERF1 and -2 are localized at the BB, where they bind NHE3 as well as the cytoskeleton, we tested whether either or both might dynamically interact with NHE3 as part of Ca^{2+} signaling. We employed FRET to study close association of NHE3 and these NHERFs and fluorescence recovery after photobleaching to monitor NHE3 mobility in the apical domain in polarized opossum kidney cells. Under basal conditions, NHERF2 and NHE3 exhibited robust FRET signaling. Within 1 min of A23187 (0.5 μM) exposure, the NHERF2-NHE3 FRET signal was abolished, and BB NHE3 mobility was transiently increased. The dynamics in FRET signal and NHE3 mobility correlated well with a change in co-precipitation of NHE3 and NHERF2 but not NHERF1. We conclude the following. 1) Under basal conditions, NHE3 closely associates with NHERF2 in opossum kidney cell microvilli. 2) Within 1 min of elevated Ca^{2+}, the close association of NHE3-NHERF2 is abolished but is re-established in ~60 min. 3) The change in NHE3-NHERF2 association is accompanied by an increased BB mobile fraction of NHE3, which contributes to inhibition of NHE3 transport activity via increased endocytosis.

Normal absorption and secretion in the gastrointestinal and renal systems are critical to maintain body water and sodium homeostasis. The BB[4] Na^+/H^+ exchanger 3 (NHE3) is responsible for the majority of electroneutral Na^+ absorption in the proximal tubule and intestine (1–5). NHE3 is rapidly stimulated and inhibited by neurohormonal substances, growth factors, and second messengers (1–5). Acute stimulation and inhibition of NHE3 is accomplished primarily by regulating the amount of NHE3 on the plasma membrane, which is determined by the balance between endocytosis and exocytosis (1–3, 6, 7).

Elevated levels of intracellular calcium inhibit NHE3 activity in intact intestine during normal digestion and in some pathophysiological conditions associated with diarrhea, such as rotovirus diarrhea (1–3, 7, 8). In a renal proximal tubule cell line, activation of adenosine A_1 receptors ($>10^{-8}$ M) inhibits NHE3 by a mechanism dependent on elevated intracellular Ca^{2+} (9). Elevated Ca^{2+} inhibition of NHE3 activity requires the NHERF2 member of the NHERF family of multi-PDZ domain-containing proteins with a permissive role for NHERF3 also demonstrated (7, 10–12).

We have recently reported that stimulation of NHE3 in polarized opossum kidney (OK) cells by LPA, which acts by increasing exocytosis, was accompanied by a transient increase in apical domain mobility of NHE3, which correlated temporally with decreased association of NHE3 and NHERF2 but not NHERF1 (13). We suggested that this change of mobility was

* This work was supported, in whole or in part, by National Institutes of Health Grants R01DK26523, RO1DK61765, PO1 DK072084, and R24DK64388 (Johns Hopkins Basic Research Digestive Diseases Development Core Center) and KO8DK088950 and T32DK2007632 from NIDDK. This work was also supported by the Johns Hopkins Center for Epithelial Biology.
[1] Both authors contributed equally to this work.
[2] Present address: Gastrointestinal Division, Albany Medical College, Albany, NY 12208.
[3] To whom correspondence should be addressed: Division of Gastroenterology and Hepatology, Dept. of Medicine, 925 Ross Research Bldg., Johns Hopkins University School of Medicine, 720 Rutland Ave., Baltimore, MD 21205-2195. Tel.: 410-955-9675; Fax: 410-955-9677; E-mail: mdonowit@jhmi.edu.

[4] The abbreviations used are: BB, brush border; NHERF, Na^+/H^+ exchanger regulatory factor; OK, opossum kidney; EGFP, enhanced GFP; BCECF, 2′,7′-bis(2-carboxyethyl)-5(6)-carboxyfluorescein; FRAP, fluorescence recovery after photobleaching; LPA, lysophosphatidic acid; CFP, cyan fluorescent protein; ROI, region of interest; TMA, tetramethylammonium.

involved in allowing the newly delivered NHE3 to be distributed over the microvilli as part of the stimulation of NHE3 activity. The purpose of this study was to determine whether similar transient dissociation of NHE3 from the apical domain NHERF proteins was part of the inhibition of NHE3 that occurs as part of stimulated endocytosis with elevation of intracellular Ca^{2+}. We hypothesized that there was likely to be a dynamic association of NHE3 with the microvillar cytoskeleton, to efficiently allow retrieval of the NHE3, which under basal conditions was mostly (~70%) fixed to the microvillar cytoskeleton (13). Here, we employed the advanced imaging techniques of FRET and FRAP, coupled to confocal microscopy, to concentrate on the apical domain events to demonstrate that NHERF2 is dynamically associated with microvillar but not intracellular NHE3. Elevation of intracellular Ca^{2+} transiently but markedly reduces NHERF2 interaction with NHE3 on the apical domain.

EXPERIMENTAL PROCEDURES

Materials—Monoclonal anti-hemagglutinin (HA) antibodies and monoclonal anti-FLAG antibodies were from Sigma. Ca^{2+} ionophore 4-Br-A23187 (nonfluorescent analog of A23187) was from Biomol (Plymouth Meeting, PA). Nigericin and 2′,7′-bis(2-carboxyethyl)-5(6)-carboxyfluorescein (BCECF) were from Molecular Probes (Eugene, OR). EZ-Link sulfo-NHS-SS-biotin and sulfo-NHS-acetate were from Thermo/Pierce. Protease inhibitor mixture (4-(2-aminoethyl) benzenesulfonyl fluoride, *trans*-epoxysuccinyl-L-leucylamido-(4-guanidino) butane (E-64), bistatin, leupeptin, aprotinin, sodium EDTA) and dynasore hydrate were from Sigma. Anti-rabbit Alexa Fluor®680 nm dye and anti-mouse IRDye™ 800 nm dye were from LI-COR (Lincoln, NE).

Construction of Expression Vectors—For the FRAP studies, full-length NHE3-EGFP cDNA with VSV-G tag epitope at the C terminus was assembled using the pEGFP-N3 vector (Clontech), as we previously described using NheI/XhoI restriction sites in-frame with the C-terminal EGFP coding sequence (14). There was an 84-bp linker between NHE3 and EGFP (ACGGAGGGCCCACCAGGCCCATACACCGACATCGAGATGAACCGGCTGGGCAAGGTCGACGGTACCGCGGGCCCGGGATCCACC). The plasmid containing YFP-GL-GPI (pEGFP-N1, Clontech) was kindly provided by K. Simons (15). For the FRET measurements, NHE3-YFP and CFP-NHERF2 were assembled using the pCS2-Venus plasmid containing the YFP (Venus) tag or the pECFP-C1 vector (Clontech) containing cerulein (CFP), respectively. Wild type full-length rabbit NHE3 with a C-terminal VSV-G in pEGFP-N3 vector was ligated with Venus using HindIII/BamHI restriction sites, creating NHE3-YFP. Wild type full-length human NHERF2 was ligated into the pECFP vector with BamHI/EcoRI restriction sites in-frame with the N-terminal enhanced CFP coding sequence, creating CFP-NHERF2. EGFP was ligated to the N terminus of NHERF2 because NHERF2 has an ERM binding domain at its C-terminal end and removing that domain (Δ30 amino acids) creates a dominant negative effect on NHE3 regulation (16). In some experiments, OK/FLAG-NHERF2/HA-NHE3 cells were used for co-precipitation because our anti-NHERF2 antibodies could not quantitatively immunodeplete NHERF2. The 3×FLAG NHERF2 construct was designed by inserting the human NHERF2 sequence into the p3×FLAG-CMV-10 expression vector (Sigma catalog no. E4401) using the HindIII and EcoRI restriction sites. The selection marker for this vector is G418 (neomycin).

Cell Culture, Transfection—OK-Tina cells, as described previously (17), were cultured on glass bottom 35-mm plastic culture dishes in DMEM/F-12 media (Invitrogen), supplemented with 10% fetal bovine serum, 100 units/ml penicillin, and 100 μg/ml streptomycin at 37 °C in a 5% CO_2, 95% air atmosphere. The intrinsic NHE3 activity in OK cells was markedly decreased by repeated applications (once per week) of the "Acid Suicide" technique (13). This resulted in OK cells with such low NHE3 endogenesis activity that the NHE3 activity after transient transfection of NHE3 was nearly all due to the transfected NHE3. These cells were then used without passaging. Post-confluent OK cells were preincubated with EGTA (3 mM, 30 min) before transfection and then transiently transfected with 10 μg of NHE3-EGFP using 10 μl of Lipofectamine 2000 (Invitrogen) according to the manufacturer's instructions and maintained in serum-free media. Studies were performed ~4 days post-confluency to allow a consistent cell population to be studied.

Cell Surface Biotinylation—NHS-SS-biotin was used to determine the percent of NHE3 on the plasma membrane per total cell NHE3 (18). OK cells stably transfected with NHERF2 and HA-NHE3 were plated on 10-cm dishes. When the cells were 100% confluent, they were serum-starved overnight before starting experiments. Cells were treated with 4-Br-A23187 (0.5 μM) for 0, 2, 10, and 30 min at 37 °C. Cells were then quickly washed with cold PBS (150 mM NaCl and 20 mM Na_2HPO_4, pH 7.4), kept at 4 °C for 40 min, and incubated with borate buffer (154 mM NaCl, 1.0 mM boric acid, 7.2 mM KCl, and 1.8 mM $CaCl_2$, pH 9.0) for 10 min. For surface labeling of HA-NHE3, cells were incubated with 0.5 mg/ml NHS-SS-biotin (Thermo/Pierce) twice for 20 min each. After labeling, cells were washed three times with quenching buffer (20 mM Tris and 120 mM NaCl, pH 7.4) to scavenge the unreacted biotin. Cells were washed three times with ice-cold PBS and solubilized with 0.8 ml of N^+ buffer (60 mM HEPES, pH 7.4, 150 mM NaCl, 3 mM KCl, 5 mM Na_3EDTA, 3 mM EGTA, and 1% Triton X-100). Lysate, representing the total post nuclear fractions, was incubated overnight with streptavidin-agarose beads. After avidin-agarose precipitation, the supernatant was retained as the intracellular fraction. The avidin-agarose beads were washed five times in N^+ buffer to remove nonspecifically bound proteins. The avidin-agarose bead-bound protein, representing apical membrane NHE3, was solubilized in equivalent volumes of loading buffer (5 mM Tris-HCl, pH 6.8, 1% SDS, 10% glycerol, 1% 2-mercaptoethanol), boiled for 5 min, size-fractionated by SDS-PAGE (10% gels), and then electrophoretically transferred to nitrocellulose. After blocking with 5% non-fat milk, the blots were probed with a monoclonal anti-HA antibody. Western analysis and the quantification of the surface fraction were performed using the Odyssey system and Odyssey software (LI-COR). Multiple volumes for each total, surface, and intracellular samples were studied, and linear regression was used to obtain a single value for each sample. Relative intensity of the surface NHE3 was compared with total NHE3

using the surface NHE3 signal/total NHE3 signal × a dilution factor for surface and total NHE3 samples and expressed as percent of total NHE3.

Co-immunoprecipitation (IP) of NHE3 with NHERF2 and NHERF1—Co-immunoprecipitation experiments were performed using cell lysates from OK/NHERF2/HA-NHE3 cells with/without 4-Br-A23187 (0.5 μM) at incubation times of 0, 2, 10, and 60 min. Cells were grown in 10-cm dishes at ~100% confluency and serum-starved overnight; cell lysates were prepared in 60 mM HEPES, pH 7.4, 150 mM NaCl, 3 mM KCl, 5 mM Na_3EDTA, 3 mM EGTA, 1 mM Na_3VO_4, and 1% Triton X-100 with protease inhibitor mixture (Sigma). Cell lysates (1.5 mg of protein/ml) were incubated overnight at 4 °C in a rotator with 30 μl of either monoclonal anti-HA affinity agarose beads (Roche Applied Science) or monoclonal anti-VSV-G antibody conjugated to agarose beads as a negative control. The beads were then gently spun down and washed five times with lysis buffer. Bound proteins were eluted with 2× sample buffer without β-mercaptoethanol to eliminate IgG. Sample buffer with β-mercaptoethanol (concentration 10%) was added back to the sample solution after elution prior to immunoblotting.

Measurement of Na^+/H^+ Exchange—Cellular Na^+/H^+ exchange activity in OK cell lines was determined fluorometrically using the intracellular pH-sensitive dye acetoxymethyl ester of BCECF-AM (5 μM; Invitrogen), as described previously (19). "TMA medium" was used to establish a base line before Na^+ exposure and contained 130 mM tetramethylammonium chloride, 5 mM KCl, 2 mM $CaCl_2$, 1 mM $MgSO_4$, 1 mM NaH_2PO_4, 25 mM glucose, and 20 mM HEPES, pH 7.4. "Na^+ medium" contained 138 mM NaCl, 5 mM KCl, 2 mM $CaCl_2$, 1 mM $MgSO_4$, 1 mM NaH_2PO_4, 25 mM glucose, and 20 mM HEPES, pH 7.4. NHE3 activity measurements under low K^+ conditions were performed with K^+-free NH_4Cl, TMA, and Na^+ solutions in which 5 mM KCl was replaced with 5 mM TMACl to maintain iso-osmolarity. To measure NHE3 activity under low K^+ conditions, the cells were preincubated with K^+-free Na^+ solution for 40 min and then incubated with BCECF with K^+-free NH_4Cl solution for 20 min. Cells were treated with/without 4-Br-A23187 (0.5 μM, 5 min). The cells were then initially perfused with K^+-free TMA solution and perfused with K^+-free Na^+ solution.

FRAP—To quantitate the lateral mobility of NHE3-EGFP at the apical domain of polarized OK cells, FRAP was used as reported previously (13, 17). OK cells were cultured on glass-bottom 35-mm plastic culture dishes in DMEM (w/o phenol red), supplemented with 10% fetal bovine serum, 100 units/ml penicillin, and 100 μg/ml streptomycin at 37 °C in a 5% CO_2, 95% air atmosphere until 100% confluent. The cells were then transfected using Lipofectamine 2000, as described previously (19), with minor revision. In this study, to increase the transfection rate, OK cells were preincubated with EGTA (3 mM, 30 min) before Lipofectamine 2000 transfection. FRAP was studied ~48 h after transfection during which time the cells were not exposed to serum.

FRAP was performed on a stage heated to 37 °C of a Zeiss LSM 410 or LSM 510/Meta confocal microscope using the 488 nm line of a 400-milliwatt Kr/Ar laser in conjunction with a ×100 Zeiss 1. 4 NA Plan Apochromat oil immersion objective, with signal collected in the OK cell apical domain (0.3-μm optical sections starting at the outer limit of the microvillus), and mobile fractions and diffusion coefficients calculated as described previously (17, 20). The Zeiss LSM software package allowed autofocusing on the coverslip surface in the reflection mode during the time lapse imaging. Fluorescence within the bleached strip was measured at a low laser power (20% power, 1% transmission) before the bleach (pre-bleach intensity) and then photobleached with full laser power (100% power, 100% transmission). Recovery was followed with low laser power at 9-s intervals, which included up to 50 images until the intensity had reached a steady plateau. The mobile fraction was determined by comparing the fluorescence intensity in the bleached region after full recovery (F) with the fluorescence intensity before bleaching (F_i) and just after bleaching (F_0). Mobile and immobile fractions were calculated by comparing the intensity ratio in regions of interest (ROI) inside and outside the bleached area just before the bleach and after recovery as described previously (21).

The postbleach intensities were normalized to correct for maximal loss of fluorescence due to the photobleach. Fluorescence intensity was normalized with prebleach intensity (F_i), which was set to 100 in each experiment. All data are shown as mean ± S.E. of the number of cells analyzed, which were obtained in at least three identical experiments, unless stated otherwise. Statistical comparison was performed by unpaired Student's t tests.

Acceptor Photobleaching Förster Resonance Energy Transfer—The acceptor photobleaching method of FRET was used to study protein-protein interactions. To perform FRET, we engineered CFP-NHERF2 and NHE3-YFP constructs. Conditions establishing that the NHE3 and NHERF2 constructs above, which were used as FRET probes, behaved similarly to wild type non-GFP-tagged proteins were reported previously (13, 22). The genetically encoded CFP and YFP variants of green fluorescent protein have become a popular donor and acceptor pair, respectively, for assessing presence of FRET. A Zeiss 510/Meta confocal microscope with an environmental chamber for temperature control, which has the FRET plus-Macro (Release 4.2; Carl Zeiss MicroImaging, Inc.) preinstalled, was used to assess the presence of FRET between CFP-NHERF2 (donor) and NHE3-YFP (acceptor) (12, 22). OK cells were transiently transfected with CFP-NHERF2 and NHE3-YFP with Lipofectamine 2000 with EGTA (3 mM, 30 min) preincubation as described in the FRAP method. ~48 h after the transfection, physiological studies were performed at 37 °C, and the cells were then kept at 4 °C for 40 min and fixed with 3% formaldehyde and mounted with Fluoro-Gel (Electron Microscopy Sciences). A Plan-NeoFluar 40×/1.3 oil immersion objective was used. Regions of interest (ROI) were selected and images collected before and after bleaching with the 514 nm laser line at maximum intensity (100%). Excitation wavelength was 458 nm for CFP and 514 nm for YFP. Emission wavelength was BP 465–510 nm for CFP and 518–561 nm for YFP.

The apparent FRET efficiency, E, was calculated as shown in Equation 1,

$$E = (I_{D\text{-post}} - I_{D\text{-pre}})/I_{D\text{-post}} \quad \text{(Eq. 1)}$$

where $I_{D\text{-}PRE}$ and $I_{D\text{-}POST}$ are the donor fluorescence intensities pre- and post-acceptor photobleaching, respectively (23). FRET efficiency was calculated by using fluorescence values that had been background-subtracted and corrected for bleaching, during acquisition, as determined from an unbleached region of interest (ROI). Statistical comparison was performed by unpaired Student's *t* tests or analysis of variance.

RESULTS

Calcium Inhibition of NHE3 Activity in Polarized OK Cells—NHE3 is acutely inhibited by elevation in the concentration of intracellular Ca^{2+} by the cholinergic agonist carbachol (24–26) as well as by serotonin (27), adenosine 1 receptor agonists (9), and thapsigargin and Ca^{2+} ionophores (18, 28, 29). Decreased NHE3 activity also occurs in PS120 fibroblasts with Ca^{2+} ionophores (10, 11). In this study, we show that intracellular Ca^{2+} elevation by Ca^{2+} ionophore 4-Br-A23187 (0.5 μM) inhibits basal NHE3 activity in NHERF2-expressing OK cells (Fig. 1*A*) (11). Ca^{2+} inhibition of NHE3 activity occurs as early as 1–2 min after 4-Br-A23187 (0.5 μM) treatment.[5] As shown in a representative experiment in Fig. 1*A*, which was repeated three times, exposure to A23187 (0.5 μM) for 5 min decreased NHE3 transport (V_{max}) activity by 41 ± 15% ($n = 3$, $p < 0.05$). In OK cells that do not endogenously contain significant amounts of NHERF2, Ca^{2+} ionophore did not alter NHE3 activity (Fig. 1*B*, $n = 3$). This confirms previous studies that demonstrated that NHERF2 was necessary for Ca^{2+} regulation of NHE3 transport activity in PS120 cells, OK cells, and Caco-2 cells (10, 11). We investigated the role in Ca^{2+} regulation of NHE3 of the ERM binding domain located in the C-terminal 30 amino acids (amino acids 307–337) of NHERF2. This was done by determining whether stably expressed NHERF2Δ30 supported the Ca^{2+} inhibition of NHE3 transport activity in OK cells. As shown in Fig. 1*C*, NHERF2Δ30 failed to reconstitute Ca^{2+} inhibition on NHE3 activity ($n = 3$). This result shows that Ca^{2+} inhibition of NHE3 activity requires the ERM binding domain of NHERF2.

The localization of NHERF2 and NHERF2Δ30 compared with NHE3 was also examined. WT NHERF2 localizes mostly in the apical plasma membrane domain in OK cells (Fig. 1*D*) where it overlaps with BB NHE3. There is no apparent overlap of NHERF2 with juxtanuclear NHE3. In contrast, NHERF2Δ30 did not localize apically, rather appearing to be entirely subapical/cytosolic with no significant overlap with BB NHE3 (Fig. 1*D*). These conclusions were supported quantitatively using software to assess overlap of NHERF2 or NHERF2Δ30 with apical or intracellular NHE3. These results suggest that Ca^{2+} inhibition of NHE3 transport activity requires binding of NHERF2 via its ERM binding domain to ezrin and to the actin cytoskeleton.

NHE3 Cell Surface Expression Is Decreased by 4-Br-A23187 in OK/NHERF2 Cells—NHE3 activity is determined by both changes in the surface expression of NHE3 and in the intrinsic NHE3 turnover number. To determine the mechanism for the Ca^{2+} inhibition on NHE3 activity, the surface amount of NHE3 with/without Ca^{2+} was quantified by cell surface biotinylation. Cell surface biotinylation was performed at 0, 2, 10, and 30 min after 4-Br-A23187 treatment to measure the time-dependent Ca^{2+}-related changes in surface amount of NHE3 in OK/NHERF2/HA-NHE3 cells. Surface amount of NHE3 decreased within 2 min after 4-Br-A23187 (0.5 μM) treatment and remained at this level for 30 min (Fig. 2). Percent of surface amount of NHE3 was normalized in each experiment to 100% at time 0. NHE3 surface/total (%) at 2, 10, and 30 min after A23187 was 73.8 ± 9.2, 73.4 ± 5.4, and 69.6 ± 11.1%, respectively ($n = 3$, all $p < 0.05$ compared with time 0).

4-Br-A23187 Transiently Increases the NHE3 Mobile Fraction in OK/NHERF2 Cells—Next, we tested the hypothesis that to allow Ca^{2+} to inhibit NHE3 activity by reducing surface NHE3, NHE3 had to be released from the microvillar cytoskeleton. In this study, FRAP was used to determine whether the Ca^{2+} inhibition of NHE3 was associated with a dynamic effect on the mobile fraction of apical NHE3. These studies were performed as follows: (*a*) after 1 h of exposure to a K^+-free medium prior to 4-Br-A231287 addition to reduce the rate of clathrin-dependent endocytosis and to allow more ready characterization of NHE3 freed from the cytoskeleton before being endocytosed (Fig. 3*A*) (30); (*b*) after exposure to dynasore (80 μM) for 30 min before ionophore addition to inhibit dynamin (Fig. 3*B*). As a control for the FRAP experiments, we demonstrated that K-free medium prevented Ca^{2+} induced inhibition of NHE3 activity (Fig. 3*A*), as did dynasore pretreatment. (Fig. 3*B*). Both K-free medium and dynasore slightly but not significantly lowered basal NHE3 activity.

FRAP was then performed before and at multiple times after A23187 addition up to 60–70 min in OK cells overexpressing NHERF2 as shown in Fig. 3, *C–E*. Fig. 3*C* is the time course with 5 min of exposure to A23187 (0.5 μM) in a single FRAP experiment with measurement starting 30 min after A23187 was initially added. Fig. 3*D* is FRAP performed starting every 10 min after A23187 exposure in a single experiment, with S.E. indicating variation in multiple ROIs from several cells in this single experiment. Fig. 3*E* shows results as mean ± S.E. from multiple experiments of results before and 30 and 60 min after initial A23187 addition. A23187 caused a significant increase in the NHE3 mobile fraction, which first became significant 10 min after A23187 addition (first time post-Ca^{2+} elevation at which FRAP was performed) (Fig. 3*D*) and returned to base line by 60 min (Fig. 3, *D* and *E*). The maximum increase in mobile fraction occurred between 20 and 30 min after A23187 addition (Fig. 3, *D* and *E*). Using this approach, the estimated NHE3 mobile fractions were as follows: (*a*) for K^+-free medium exposure, 45 ± 3% for control conditions, 81 ± 7% at 30 min, and 29 ± 8% at 60 min after A23187; (*b*) for dynasore-exposed cells, 45 ± 7% for control conditions, 90 ± 2% at 30 min, and 38 ± 11% at 60 min after A23187 (Fig. 3*E*).

A23187 has no effect on NHE3 activity in OK cells that lack NHERF2 expression (Fig. 1). We also previously showed that there are two different pools of NHE3 on the OK apical plasma membrane, a mobile and an immobile pool, the latter limited by binding to PDZ domain-containing proteins (17). Therefore, we asked whether the Ca^{2+} stimulatory effect on NHE3 mobility also required NHERF2. FRAP was performed on OK cells

[5] N. C. Zachos, R. Sarker, and M. Donowitz, unpublished data.

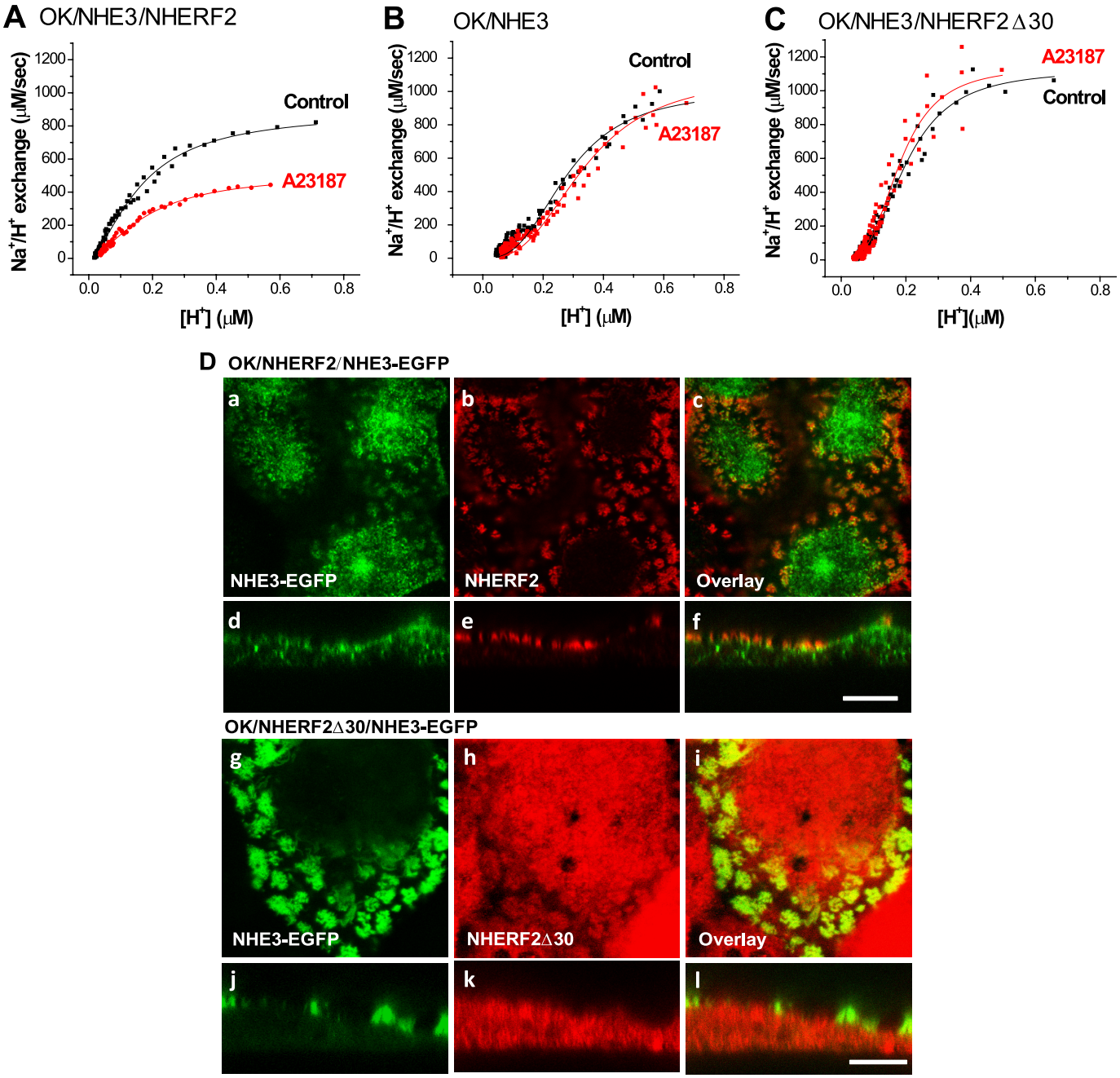

FIGURE 1. **Elevated Ca^{2+} inhibits basal NHE3 activity in OK/NHERF2/HA-NHE3 cells but not in OK/HA-NHE3 or OK/NHERF2Δ30/HA-NHE3 cells.** NHE3 activity (ΔpH_i/min) was measured by using the BCECF/fluorometer method starting 5 min after exposure to Ca^{2+} ionophore 4-Br-A23187 (0.5 μM). *A,* Ca^{2+} ionophore inhibits basal NHE3 activity (V_{max}) in OK/HA-NHE3 cells stably transfected with NHERF2. *B,* there was no effect of 4-Br-A23187 in cells without exogenous NHERF2. *C,* 4-Br-A23187 failed to inhibit NHE3 activity in OK/HA-NHE3 cells stably transfected with NHERF2Δ30. The results shown in *A–C* are from single representative experiments, with similar results in three experiments in each of *A–C*. *D,* intracellular location of NHERF2Δ30 fails to co-localize with NHE3-EGFP in OK cells, although there is more overlap with NHERF2. NHE3-EGFP was transiently transfected in OK cells stably transfected with NHERF2 (*panels a–f*) or NHERF2Δ30 (*panels g–l*). Cells were fixed with 3% formaldehyde. NHE3 was detected by fluorescence (*panels a* and *d* and *panels g* and *j*), and NHERF2 (*panels b* and *e*) or NHERF2Δ30 (*panels h* and *k*) was detected by anti-NHERF2 antibody (α-2570). Overlay images are in (*panels c* and *f* and *panels i* and *l*). *Bar,* 10 μm. Images were obtained by LSM 510 confocal microscopy.

lacking exogenous NHERF2. In the absence of NHERF2, the Ca^{2+}-stimulatory effects on NHE3 mobility did not occur (Fig. 3*F*). NHE3 mobile fractions of OK cells lacking NHERF2 were 65.5 ± 2.8% for the control and 63.3 ± 3.6% after 4-Br-A23187 (0.5 μM; 30 min). The increase in basal NHE3 mobile fraction in the absence of NHERF2 is as discussed previously (17). These results show that the Ca^{2+}-stimulatory effect on both the NHE3 mobile fraction and NHE3 transport activity requires NHERF2.

NHERF2 but Not NHERF1 Dynamically Co-precipitates with NHE3 with Elevated Ca^{2+}—Previous FRAP studies have shown that NHERF2 is required for the dynamic increase in apical NHE3 mobility that occurs in OK cells with LPA and D-glucose stimulation of NHE3 activity (13, 22). Both the LPA- and D-glucose-induced increases in NHE3 mobility were associated with dynamic physical association of NHE3 and NHERF2 as indicated by basal co-precipitation of NHE3 and NHERF2, followed

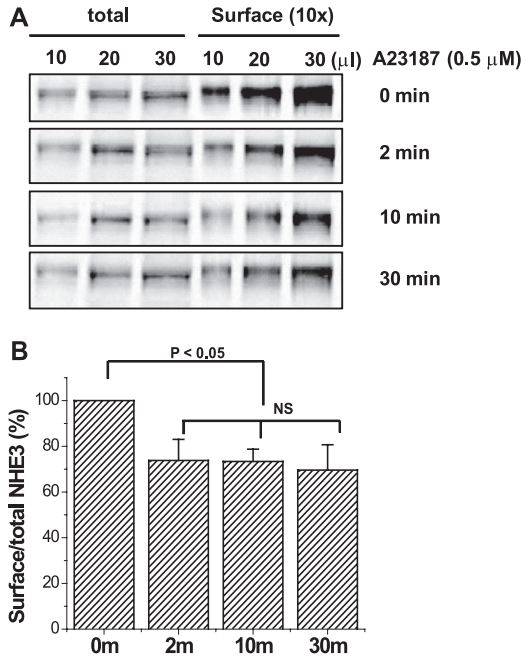

FIGURE 2. **Elevated Ca^{2+} (ionophore 4-Br-A23187) caused a rapid and prolonged decrease in NHE3 surface expression.** *A,* OK/NHERF2/HA-NHE3 cells were treated with 4-Br-A23187 (0.5 μM) for 0, 2, 10, and 30 min at 37 °C in a 5% CO_2, 95% air atmosphere, and the cells were then quickly washed with cold PBS three times (4 °C) and kept at 4 °C for 30 min. Cells were then biotinylated, and the total lysate was collected in 1 ml. The surface-biotinylated proteins were collected by avidin precipitation (surface) and retrieved in 0.1 ml of sample buffer. The NHE3 protein was loaded into each lane with the same volume in a series of dilutions (10, 20, and 30 μl), which were detected by monoclonal anti-HA antibody. Results from a single experiment are shown. *B,* results from three experiments as in *A* are shown as mean ± S.E. In each experiment, results were normalized with time 0 set as 100%. *p* values are compared with untreated control (paired *t* test). *NS*, not significant.

by a transient period where there was no co-precipitation (13, 22). We thus hypothesized that down-regulation of NHE3 activity by 4-Br-A23187 might be associated with dynamic interaction between NHE3 and NHERF2 and/or NHERF1, presumably to free up BB NHE3 for endocytosis. We performed co-immunoprecipitation experiments using OK cells stably transfected with HA-NHE3 and FLAG-NHERF2 or FLAG-NHERF1. NHE3 was effectively co-precipitated with NHERF2 at time 0 min (without 4-Br-A23187). However, 2 and 10 min after A23187 (0.5 μM) treatment, NHERF2 failed to co-precipitate NHE3 (Fig. 4*A*). By 60 min the association of NHE3 and NHERF2 had been re-established, as shown in Fig. 4*A*. In contrast, 4-Br-A23187 treatment had no effect on the co-precipitation of NHE3 with NHERF1 over the same time course (Fig. 4*B*). These data suggest that the Ca^{2+} increase of the BB NHE3 mobile fraction depends on NHERF2 association with NHE3, which is transiently reduced by elevation of Ca^{2+}.

Monitoring Dynamic Interaction between NHERF2 and NHE3 in the OK Cell Apical Domain by FRET—To define the spatial and temporal resolution of the interaction of NHE3 and NHERF2 in the OK apical domain upon Ca^{2+} mobilization, we employed the FRET technique. The FRET constructs were made by tagging YFP to the NHE3 C terminus and CFP to the N terminus in NHERF2 (Fig. 5*A*). CFP-NHERF2 and NHE3-YFP were transiently transfected into polarized OK cells. The CFP-NHERF2 was primarily present in microvilli of OK cells, as shown in Fig. 5*B*. NHE3-YFP had two locations, on the microvilli and in the juxtanuclear domain in OK cells, as reported previously (17, 22). The FRET signal was detected by an acceptor photo-bleaching strategy (Fig. 6). FRET efficiency was calculated as described in following method: (%FRET = (intensity of ROI (post-bleaching) − intensity of ROI (pre-bleaching))/intensity of ROI (post-bleaching). The principle of this technique is to photo-bleach the YFP (acceptor) to reduce energy transfer between CFP (donor) and YFP, which is the parameter indicating whether there is any interaction between the NHE3-YFP/CFP-NHERF2 FRET pair. Under control conditions, both NHE3-YFP and CFP-NHERF2 co-localized predominantly at microvilli, whereas NHE3-YFP was also in the juxtanuclear area (Fig. 5*B*). The CFP and YFP fluorescent signals were acquired before and after photo-bleaching, as shown in Fig. 6*A*. Five min of exposure to 514 nm light almost completely bleached the YFP fluorescent signal, which, oppositely, increased the CFP signal. These data reveal that energy transfer occurs between YFP-NHE3 and CFP-NHERF2 under basal conditions consistent with a direct physical interaction or very close approximation between NHE3 and NHERF2 under basal conditions.

To further confirm that the FRET signaling was from the NHE3 and NHERF2 interaction, we employed YFP-GL-GPI, a protein present only in the outer plasma membrane, as a negative control (Fig. 6*C*) (15). Under the same conditions, as shown in Fig. 6*A* when YFP-GL-GPI was bleached, there was no increase in CFP-NHERF2 signaling, reinforcing that FRET signaling in Fig. 6*A* is from the interaction of NHE3 and NHERF2.

FRET intensity was quantified in fixed cells. FRET signaling in OK/NHERF2 cells co-transfected with YFP-GL-GPI was approximately −5–10%, presumably because of CFP photobleaching (Fig. 6, *C* and *D*). In OK/NHERF2/NHE3 cells, there was ~10% FRET signaling (Fig. 6, *A* and *D*). Taking the CFP photobleaching into account, the FRET between NHE3 and NHERF2 was ~15–20%.

Elevated Intracellular Ca^{2+} Reduces the Interaction of NHE3 and NHERF2 at Microvilli by FRET—The co-immunoprecipitation studies revealed that the interaction of NHE3 and NHERF2 is down-regulated by elevated intracellular calcium (Fig. 4*A*). We therefore used FRET to monitor the effect of calcium on these interactions at the OK cell microvilli. The polarized OK cells stably transfected with YFP-NHE3 and CFP-NHERF2 were first treated with 4-Br-A23187 for 1 min at 37 °C, followed by fixation in 3% formaldehyde. The fixed cells then had FRET measured by acceptor photobleaching. The FRET signaling was markedly reduced at the microvilli ~1 min after Ca^{2+} elevation to ~3%, consistent with almost total dissociation of NHE3 and NHERF2 or a change in their relative locations (Fig. 6, *B* and *D*). These data demonstrate a rapid regulated dissociation of NHE3 and NHERF2 at the apical membrane of epithelial cells after Ca^{2+} is increased.

DISCUSSION

The major conclusion from this study is that there are two components of acute NHE3 inhibition by elevated Ca^{2+} in polarized renal proximal tubule epithelial cells. These are the previously characterized stimulated endocytosis (7) and the

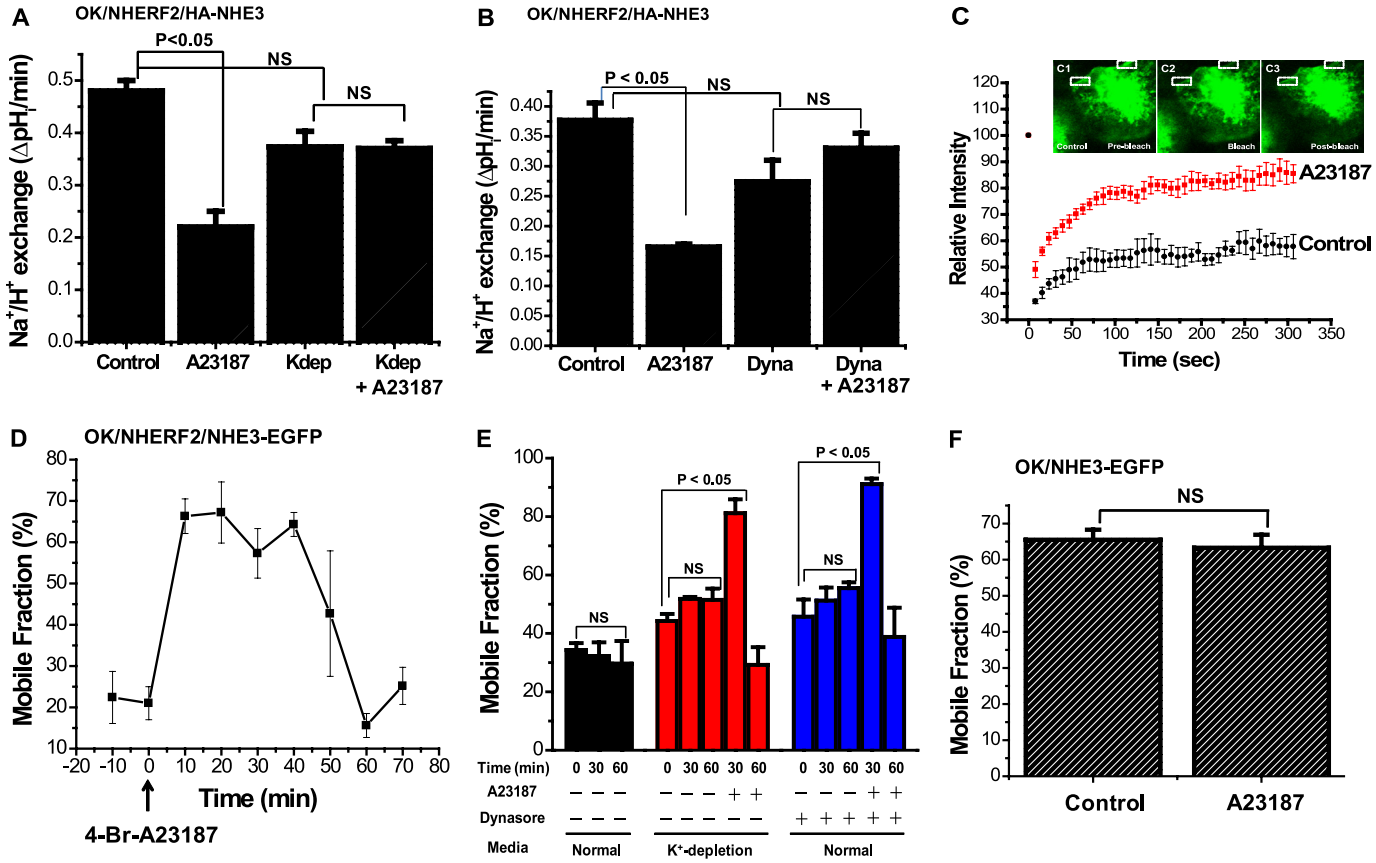

FIGURE 3. **Acute elevation of Ca^{2+} dynamically increases the lateral mobility of NHE3 determined by FRAP in the apical domain of OK cells.** *A*, 4-Br-A23187 inhibition of NHE3 activity does not occur with exposure to K^+-deficient medium. Exposure to K^+-deficient medium (142 mM NaCl, 1 mM $CaCl_2$, 1 mM $MgCl_2$, 20 mM HEPES, pH 7.4, pH adjusted with Tris) was for 1 h before transport measurements. K^+-deficient medium caused a slight but not significant decrease in basal NHE3 activity. Results shown are mean ± S.E. from three experiments. *p* values are paired *t* tests. *B*, dynasore pretreatment (80 μM, 30 min) slightly but not significantly lowered basal NHE3 activity and prevented A23187 inhibition of NHE3. Results are mean ± S.E. from three experiments. *p* values are paired *t* test. *C*, FRAP studies of NHE3 were performed on OK/NHERF2 cells transiently transfected with NHE3-EGFP with/without (control) 4-Br-A23187 (0.5 μM) starting 30 min after A23187 exposure. Relative fluorescence intensity after photo-bleaching was measured for 300 s. K^+-deficient medium, as above, was used to reduce endocytosis induced by elevated Ca^{2+} (30). *Inset* images show NHE3-EGFP pre-bleaching (*C1*), immediately post-bleaching (*C2*), and after recovery (300 s) (*C3*) in studies performed 30 min after A23187 exposure. *D*, elevated Ca^{2+} transiently increased NHE3-EGFP mobility in OK/NHERF2/NHE3-EGFP cells. FRAP was performed before and at various times after 4-Br-A23187 addition to measure BB lateral mobility of NHE3-EGFP in OK cells. This was done with K^+-deficient medium pretreatment for 1 h and throughout the experiment. Minutes after A23187 addition when FRAP studies were performed is shown on the *x* axis. Results of a typical experiment are shown with mean ± S.E. shown for ROIs from this single experiment to show the variability with at least three ROIs from >1 cell analyzed. *E*, Ca^{2+} elevation via A23187 transiently stimulates NHE3 mobile fraction at 30 min, which then returns to base line at 60 min under K^+-deficient conditions as well as with dynasore (80 μM, 30 min) treatment. Basal NHE3 mobile fraction with normal medium or K^+-deficient medium or dynasore without 4-Br-A23187 did not change significantly over the time of the experiments. Similar results were found with both K^+-deficient media exposure and dynasore. The mean ± S.E. were calculated from three independent experiments. *p* values are in comparison to zero time (paired *t* test). *F*, A23187 did not alter the NHE3 mobile fraction 30 min after A23187 addition in the absence of NHERF2. Study was done with K^+-deficient medium as in *D*. Results are mean ± S.E. of 30-min time point from three experiments. *NS*, not significant.

newly recognized dynamic dissociation of NHE3 from the cytoskeleton, which occurs via rapid but transient release of NHE3 from the apical domain NHERF2 and the apical cytoskeleton. The latter occurs in the absence of increased endocytosis of NHE3 as indicated by its occurrence when NHE3 endocytosis was reduced by K^+ depletion or exposure to the dynamin inhibitor dynasore. We propose, but have not proven, that the latter is a necessary step to mobilize the pool(s) of NHE3 in the microvilli which is acutely internalized in response to elevated Ca^{2+} and includes some of the microvillar NHE3, which associates with NHERF2 under basal conditions (Fig. 7).

We previously showed that there was similar dissociation of NHE3 from the microvillar cytoskeleton and NHERF2 and increased NHE3 apical membrane mobility as part of acute stimulation of NHE3 by exocytosis from the recycling system in OK cells in response to LPA and in Caco-2 cells in response to luminal D-glucose (13, 22). This was hypothesized as being necessary to spread the exocytosed NHE3 over the microvillar surface. The importance of the observation that both acute stimulation and inhibition of NHE3 involve regulation of NHE3 association with the apical domain cytoskeleton, as well as in trafficking, adds complexity to understanding regulated transport. To understand regulation of intestinal and renal proximal tubule Na^+ absorption, signaling that affects both apical trafficking and microvillar cytoskeleton association of NHE3 must be considered. Likely, but not proven, is that this two-component regulation that involves transporter/microvillar cytoskeleton association also is relevant for multiple other plasma membrane transport proteins in addition to NHE3.

The use of this Ca^{2+} ionophore-based model of Ca^{2+}-induced NHE3 inhibition requires comment given that elevated Ca^{2+} is known to be necessary for both endocytosis and exocy-

tosis; the latter at least partially based on the Ca^{2+} dependence of synaptotagmin, which is thought to be the final step of membrane fusion of exocytosis (31). Agonists that elevate cytosol-free Ca^{2+} can be separated into two groups as follows. 1) Inhibitors of NHE3, include serotonin (27), carbachol (11, 24–26), adenosine type 1 receptors (9, 32), and thapsigargin and Ca^{2+} ionophores, including 4-Br-A23187 in cells expressing NHERF2 or NHERF3 (12, 18, 28) as used in this study. 2) Stimulators of NHE3 include LPA (32, 33), low concentrations of angiotensin II (34), A23187 in the presence of NHERF4 (35), and EGF.[6] One way to separate these effects appears to be that the effects of the inhibitors of NHE3 can be blocked by PKC antagonists. This is true for adenosine type 1 receptors, serotonin (27), carbachol (31), and ionophores in the presence of NHERF2 and NHERF3 and not for LPA (33), angiotensin (34), and ionophore in the presence of NHERF4.[6] Thus, this ionophore model of Ca^{2+}-induced NHE3 inhibition, which has been shown to be associated with stimulated endocytosis, is not the same model as our previously reported LPA stimulation of NHE3 activity, in which the elevation in intracellular Ca^{2+} was necessary for the NHE3 stimulation. However, together they show that this two-component regulation is relevant to both stimulated endocytosis and exocytosis.

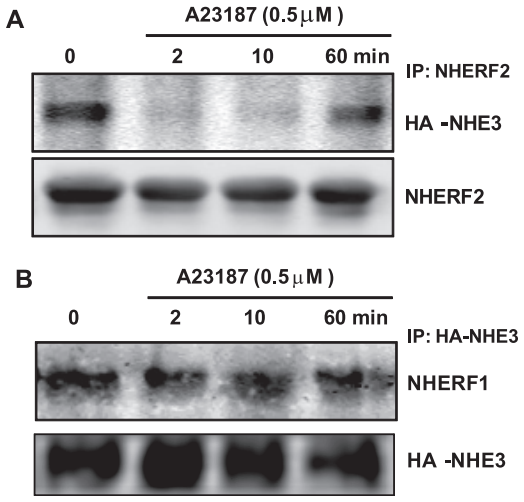

FIGURE 4. **A23187 effects on co-precipitation of NHE3 and NHERF2 but not NHERF1 in OK cells are dynamic.** *A,* OK/FLAG-NHERF2/HA-NHE3 cells were exposed to 4-Br-A23187 (0.5 μM) for 0, 2, 10, and 60 min, washed with chilled PBS (4 °C), and then kept at 4 °C for 30 min. Total cell lysate was then prepared for immunoprecipitation (*IP*). FLAG-NHERF2 was immunoprecipitated using anti-FLAG antibody, and the co-precipitated HA-NHE3 was detected by immunoblotting with anti-HA antibody. NHERF2 failed to co-precipitate NHE3 2 and 10 min after 4-Br-A23187 but co-precipitated NHE3 before and 60 min after A23187 exposure. A single experiment is shown that was performed three times with similar results. *B,* experiments as in *A* were performed using OK/FLAG-NHERF1/HA-NHE3 cells. NHE3 was immunoprecipitated, and similar amounts of NHERF1 were co-precipitated before and 2, 10, and 60 min after A23187. Similar results were found in four experiments.

The model of acute Ca^{2+}-induced inhibition of NHE3 activity using a Ca^{2+} ionophore was selected to bypass plasma membrane receptors to allow evaluation of rapid events downstream of this second messenger on NHE3 mobility and the physical interactions of NHE3 with several other proteins. Elevated Ca^{2+} reduced BB NHE3 amount and inhibited NHE3 activity with effects detectable by the techniques used here at the earliest time points studied (5–10 min after ionophore addition). This rapid response had been seen by us previously in Caco-2 cells with marked reduction with BB NHE3 amount within 2 min of carbachol exposure as assessed by total internal reflection (TIRF) microscopy (7). The dissociation of NHE3 and NHERF2 occurred within 1–2 min of Ca^{2+} elevation as deter-

[6] R. Sarker, N. C. Zachos, and M. Donowitz, unpublished data.

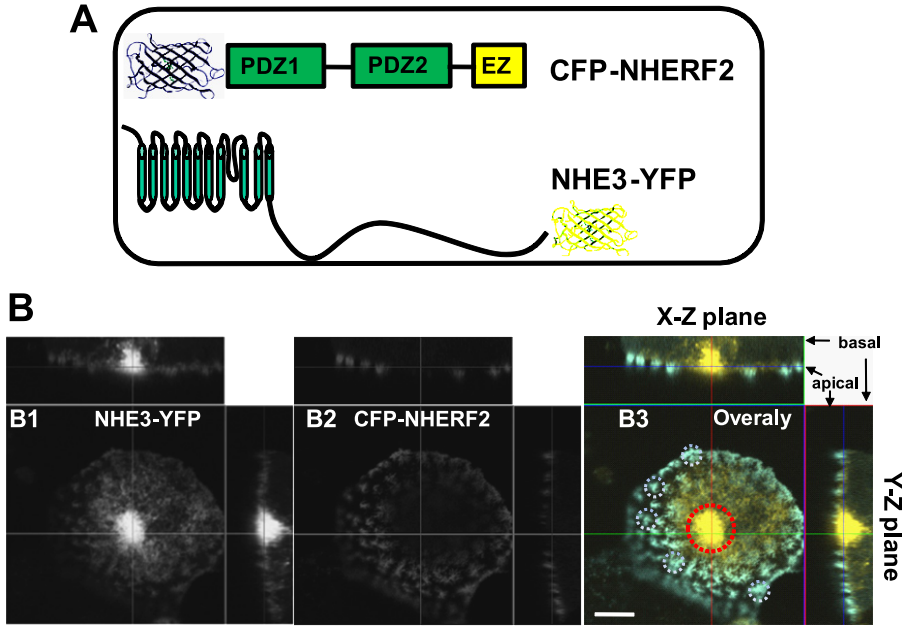

FIGURE 5. **Expression of FRET pair NHE3-YFP and CFP-NHERF2 in the microvilli.** *A,* FRET pair was CFP-tagged N terminus of NHERF2 and YFP-tagged C terminus of NHE3. NHE3-YFP and CFP-NHERF2 were transiently transfected into the OK cells. *B,* confocal images were collected from NHE3-YFP (*panel B1*), CFP-NHERF2 (*panel B2*), and merge (*Blue,* CFP-NHERF2; *green,* NHE3-YFP) (*panel B3*). Microvilli and the juxtanuclear area of polarized OK cells were marked as ROIs with the *white circles* and the *red circle*, respectively (*panel B3*). CFP-NHERF2 was mostly localized on the microvilli (representative *white circles*), and NHE3-YFP was localized to both the microvilli (*white circles*) and intracellular juxtanuclear compartment (*red circle*). *Bar,* 10 μm. Images were obtained by LSM 510 confocal microscopy of OK cells grown on glass coverslips.

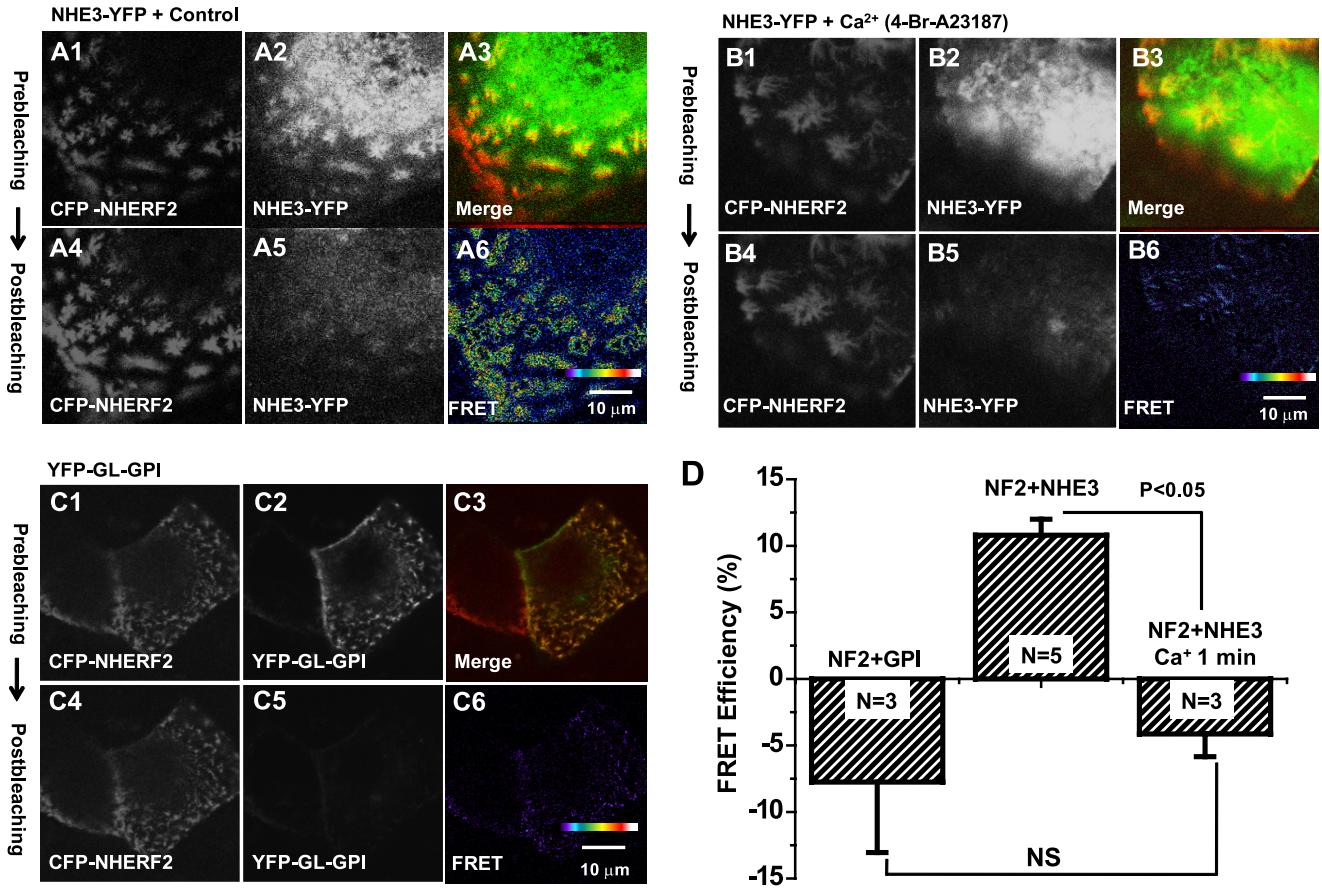

FIGURE 6. **Ca^{2+} regulates dynamic interaction of NHE3 and NHERF2 at microvilli revealed by FRET.** *A, in vivo* detection of interaction of NHE3-YFP and CFP-NHERF2 in the apical domain by acceptor photobleaching FRET under basal conditions. Images were acquired before (*top panels, panel A1* (*CFP-NHERF2*); *panel A2* (*NHE3-YFP*); *panel A3* (*Merge*)), and after (*bottom panels, panel A4* (*CFP-NHERF2*); *panel A5* (*NHE3-YFP*)) photobleaching of NHE3-YFP. *Panel A6* shows FRET image (pseudo-colored). Results in *panels A1, 2, 4,* and *5* are converted gray scale images. *Panel A3* shows collected *red-green* image to indicate overlap of NHE3/NHERF2. FRET images (*panels A6, B6,* and *C6*) were acquired by MetaMorph image analysis software by using the FRET formula, $E = (I_{D\text{-}post} - I_{D\text{-}pre})/I$, where $I_{D\text{-}pre}$ and $I_{D\text{-}post}$ are the donor fluorescence intensities pre- and post-acceptor photobleaching, respectively. *B,* elevated intracellular Ca^{2+} completely abolished the FRET signal within 1 min. The cells were treated with 4-Br-A23187 (0.5 μM) for 1 min at 37 °C and then fixed with 3% formaldehyde prior to imaging. Images were acquired before (*top panels*: *panel B1* (*CFP-NHERF2*); *panel B2* (*NHE3-YFP*); *panel B3* (*Merge*)) and 1 min after (*bottom panels*: *panel B4* (*CFP-NHERF2*); *panel B5* (*NHE3-YFP*)) photobleaching of NHE3-YFP. *Panel B6* shows FRET image. *C,* YFP-GL-GPI was used as a negative control. Images were acquired before (*top panels*: *panel C1* (*CFP-NHERF2*); *panel C2* (*YFP-GL-GP*); *panel C3* (*Merge*) and after (the *bottom panel*: *panel C4* (*CFP-NHERF2*); *panel C5* (*YFP-GL-GPI*)) photobleaching of YFP-GL-GPI. *Panel C6* shows FRET image. *D,* quantitation from *A* to *C* was performed as under "Experimental Procedures" and is shown as means ± S.E. in a *bar graph* representation from the above experiments. FRET efficiency (%) at the microvilli was quantified from an average of 10 ROIs per cell from 10 individual cells. *N* refers to number of separate experiments. *p* values are unpaired *t* test. FRET was observed between NHE3 and NHERF2 (*NF2*). Ca^{2+} ionophore 4-Br-A23187 (0.5 μM) completely abolished FRET signals within 1 min. *NS,* not significant.

mined by FRET and co-precipitation, and thus both changes in NHE3 endocytosis and NHERF2 association occur over a similar time course indicating the need for coordination of these two events but not allowing determination of which comes first. Future studies will examine whether receptor-related inhibition of NHE3 by Ca^{2+}-dependent mechanisms affects NHE3/cytoskeletal association in the microvillus independently of changes in intracellular Ca^{2+}.

Because not all microvillar NHE3 is either endocytosed or mobilized with elevated Ca^{2+} (Figs. 1–3) implies that there are multiple BB pools of NHE3, only some of which are involved in this aspect of NHE3 regulation. NHE3 has been shown by several techniques to be present in multiple pools in the apical domain of epithelial cells, as well as intracellularly (1, 3, 36, 37). The apical pools have been defined in multiple ways, with no clear assignment of characteristics to the pools to allow each to be related to the others. These apical domain pools of NHE3 have been characterized as follows: 1) Mobile *versus* immobile pools in the BB, defined by fluorescence recovery after photobleaching as examined in this study and others (17, 22, 38, 39). As shown here, ~70% of OK cell apical membrane NHE3 is immobile, whereas 30% is mobile in cells expressing NHERF1 and -2. 2) Presence in lipid rafts *versus* non-lipid raft (39–41). 3) Megalin-associated *versus* not megalin-associated, with the latter on the microvilli and able to transport NHE3 and the former thought to reside in the inter-microvillus space and lack NHE3 activity (42). To better understand the nature of the Ca^{2+}-induced dynamically mobilized BB pool of NHE3, as well as that endocytosed, will require at least applying all the above criteria simultaneously to more fully define the pools of BB. Our study adds that the NHERF1-binding pool of microvillar NHE3 is not responsive to short term changes in NHE3 activity that occur via stimulated endocytosis from elevated Ca^{2+}. We previously demonstrated that in Caco-2 cells NHERF3 is present in the outer aspects of the microvilli, where it overlaps with NHERF1

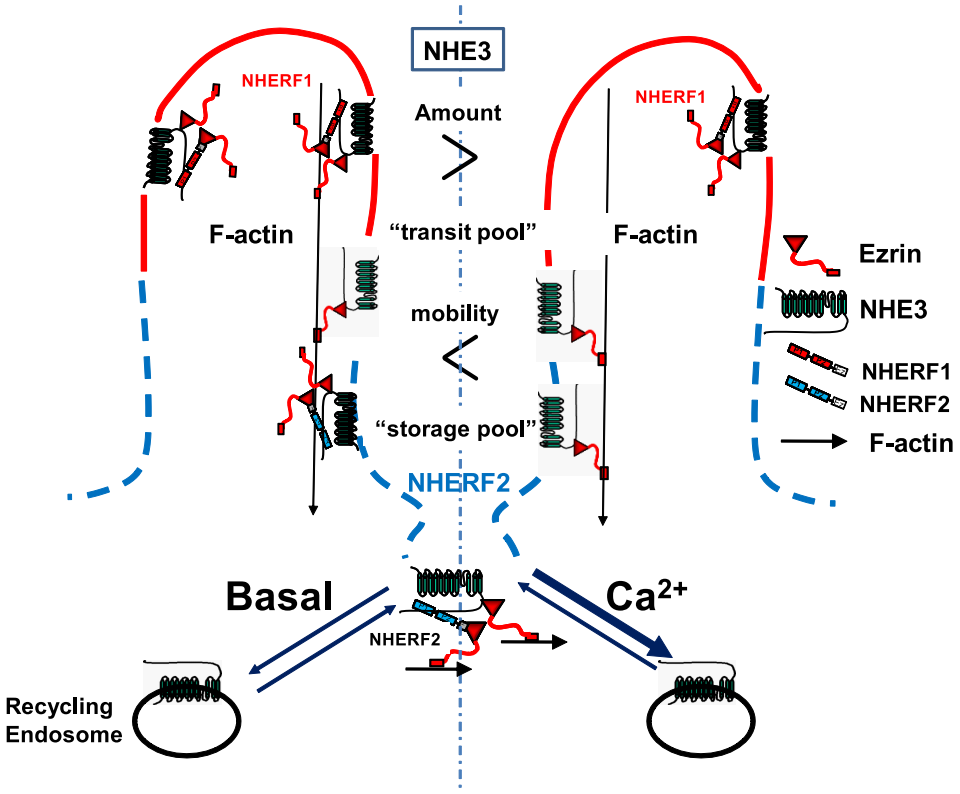

FIGURE 7. **Proposed model for NHE3 transit pool and "storage pool" in OK cell apical domain with Ca^{2+}-induced dissociation of NHE3 from NHERF2.** NHERF2 and a pool of apical NHE3 co-localize in OK cells under basal conditions, and some NHE3 co-precipitates with NHERF2. The amount of NHE3 that is immobile (fixed to the microvillar cytoskeleton) decreases within 10 min of Ca^{2+} elevation (FRAP) and NHE3 and NHERF2 dissociate by 1–2 min (FRET, co-precipitation). We assume but have not proved that the freed up NHE3 is at least part of the apical pool of NHE3 that is endocytosed in response to elevated Ca^{2+}. Note that the lack of dissociation of NHE3-NHERF1 with elevated Ca^{2+} identifies a Ca^{2+}-insensitive pool of NHE3 present in the microvilli. NHE3 that binds NHERF2 defines both the pool of NHE3 stored in the apical domain under basal conditions (storage pool), which is likely to be inactive, and the transit pool of NHE3, which moves from the microvillus to the inter-microvillus clefts as part of stimulated endocytosis.

and is necessary for Ca^{2+}-dependent inhibition of NHE3. NHERF3 undergoes a dynamic, time-limited dissociation from NHE3 with elevated Ca^{2+} (12). We hypothesize that the NHERF3-NHE3 association may further define the dynamic microvillar pool that provides the NHE3 for endocytosis.

We have suggested that the role of NHERF2 in setting NHE3 activity in polarized Na^+-absorptive cells involves establishing a storage pool of NHE3 in the apical domain of these cells (13, 22). When NHERF2 is knocked down in Caco-2 cells, the basal activity of NHE3 is increased as is the amount of NHE3 in the apical domain as indicated by co-localization with apically added wheat germ agglutinin (at 4 °C) and access to apical biotin (at 4 °C) (22). We suspect that this pool of NHE3 becomes a "transit pool" as part of signaling (17, 22). The dynamic release of NHE3 from NHERF2 and increase in apical domain mobility of NHE3 with A23187 exposure is likely to be similarly involved with allowing the microvillar NHE3 to move to the inter-microvillus space as part of stimulated endocytosis. Based on the D-glucose and the LPA studies of *stimulated* NHE3 activity and Ca^{2+}-*inhibited* NHE3 activity described here, in all of which there is physical dissociation of NHE3 and NHERF2, we suggest that the NHE3 which associates with NHERF2 (Fig. 7) in the OK cell apical domain is "stored" to provide a pool to become mobilized for stimulated endocytosis or is mixed with newly delivered NHE3 via stimulated exocytosis to spread over the microvillus (13, 22). Under basal conditions, this NHE3/NHERF2 pool is in the lower microvillus, inter-microvillus cleft, and/or terminal web area (12, 17, 22, 43). In OK and Caco-2 cells, this NHE3 storage pool appears to be in all these apical domains, whereas in the renal proximal tubule this pool of NHE3 co-localizes with megalin at or just above the inter-microvillus cleft area (44, 45). Whether the storage pool of NHE3 is the same in Caco-2 and OK cells and in proximal tubules is not known.

The role of NHERF2 in Ca^{2+}-dependent inhibition of NHE3 has only been partially clarified. The NHERF2 dependence requires the NHERF2 C-terminal 30 amino acids, which is used to bind to the actin cytoskeleton via ezrin (Fig. 7). When NHERF2 Δ30 was expressed in OK cells compared with NHERF2, the NHERF2 Δ30 was not present in the BB and rather seemed to be subapical (Fig. 1*D*). This indicates that not only does NHERF2 establish the location of NHE3 in the apical domain (22) but also that the binding of NHERF2 to the actin cytoskeleton via binding ezrin is necessary for the NHERF2 BB localization. It is not known if just binding ezrin without binding NHE3 or other BB binding partners is sufficient to localize NHERF2 to the BB.

NHE3 returns to its fixed state in the OK cell apical domain within 60 min of elevation of Ca^{2+}. It is assumed that the ionophore leads to prolonged Ca^{2+} elevation, and the effect to inhibit NHE3 activity persists, although with prolonged ionophore exposure the issue of cell damage must be considered.

This time limitation in the dynamic NHE3-NHERF2 association, as seen with the Ca^{2+} effect on the NHE3 mobile fraction, also occurred with the LPA-induced increase in the NHE3 mobile fraction (13). By 50 min of LPA exposure, the NHE3 mobile fraction had returned to its initial fixed state, even though the NHE3 activity and percent NHE3 present on the BB were both still increased. This return to base-line mobile fraction with both LPA-stimulated and elevated Ca^{2+}-inhibited NHE3 was associated with a return to basal interactions between NHE3 and NHERF2, as indicated by co-precipitation. What leads to the reversal of both phenomena, although changes in NHE3 transport activity persist, is not known. We suggest signaling is initiated by the LPA and Ca^{2+} ionophore that leads to the reassociation of NHE3 and NHERF2, but the nature of the signal has not been identified.

In summary, our studies used the advanced imaging approaches FRET and FRAP to reveal that NHE3 and NHERF2 dynamically interact at the microvilli of polarized OK cells. Elevation of intracellular Ca^{2+} causes rapid dissociation of NHE3 from NHERF2, presumably to allow subsequent NHE3 endocytosis, thus decreasing the surface NHE3 amount and NHE3 activity, as observed here. This dissociation is time-limited with physical association of NHE3 and NHERF2 being re-established by an unknown signaling mechanism. As we reported with LPA stimulation of NHE3, the signaling that regulates Ca^{2+}-induced inhibition of NHE3 must be thought of as affecting both changes in trafficking (Ca^{2+}-induced endocytosis) and regulation of NHE3 association with the microvillar cytoskeleton, with understanding the coordination of the events remaining to be clarified.

REFERENCES

1. Donowitz, M., and Li, X. (2007) *Physiol. Rev.* **87,** 825–872
2. Zachos, N. C., Tse, M., and Donowitz, M. (2005) *Annu. Rev. Physiol.* **67,** 411–443
3. Donowitz, M., Mohan, S., Zhu, C. X., Chen, T. E., Lin, R., Cha, B., Zachos, N. C., Murtazina, R., Sarker, R., and Li, X. (2009) *J. Exp. Biol.* **212,** 1638–1646
4. Bobulescu, I. A., and Moe, O. W. (2009) *Pflugers Arch.* **458,** 5–21
5. Bobulescu, I. A., and Moe, O. W. (2006) *Semin. Nephrol.* **26,** 334–344
6. Orlowski, J., and Grinstein, S. (2004) *Pflugers Arch.* **447,** 549–565
7. Zachos, N. C., Kovbasnjuk, O., and Donowitz, M. (2009) *Ann. N.Y. Acad. Sci.* **1165,** 240–248
8. Morris, A. P., and Estes, M. K. (2001) *Am. J. Physiol. Gastrointest. Liver Physiol.* **281,** G303–G310
9. Di Sole, F., Cerull, R., Petzke, S., Casavola, V., Burckhardt, G., and Helmle-Kolb, C. (2003) *J. Am. Soc. Nephrol.* **14,** 1720–1730
10. Kim, J. H., Lee-Kwon, W., Park, J. B., Ryu, S. H., Yun, C. H., and Donowitz, M. (2002) *J. Biol. Chem.* **277,** 23714–23724
11. Lee-Kwon, W., Kim, J. H., Choi, J. W., Kawano, K., Cha, B., Dartt, D. A., Zoukhri, D., and Donowitz, M. (2003) *Am. J. Physiol. Cell Physiol.* **285,** C1527–C1536
12. Zachos, N. C., Li, X., Kovbasnjuk, O., Hogema, B., Sarker, R., Lee, L. J., Li, M., de Jonge, H., and Donowitz, M. (2009) *J. Biol. Chem.* **284,** 23708–23718
13. Cha, B., Zhu, X. C., Chen, W., Jones, M., Ryoo, S., Zachos, N. C., Chen, T. E., Lin, R., Sarker, R., Kenworthy, A. K., Tse, M., Kovbasnjuk, O., and Donowitz, M. (2010) *J. Cell Sci.* **123,** 2434–2443
14. Janecki, A. J., Janecki, M., Akhter, S., and Donowitz, M. (2000) *J. Biol. Chem.* **275,** 8133–8142
15. Keller, P., Toomre, D., Díaz, E., White, J., and Simons, K. (2001) *Nat. Cell Biol.* **3,** 140–149
16. Weinman, E. J., Steplock, D., Wade, J. B., and Shenolikar, S. (2001) *Am. J. Physiol. Renal Physiol.* **281,** F374–F380
17. Cha, B., Kenworthy, A., Murtazina, R., and Donowitz, M. (2004) *J. Cell Sci.* **117,** 3353–3365
18. Sarker, R., Grønborg, M., Cha, B., Mohan, S., Chen, Y., Pandey, A., Litchfield, D., Donowitz, M., and Li, X. (2008) *Mol. Biol. Cell* **19,** 3859–3870
19. Levine, S. A., Nath, S. K., Yun, C. H., Yip, J. W., Montrose, M., Donowitz, M., and Tse, C. M. (1995) *J. Biol. Chem.* **270,** 13716–13725
20. Kenworthy, A. K., and Edidin, M. (1998) *J. Cell Biol.* **142,** 69–84
21. Ellenberg, J., Siggia, E. D., Moreira, J. E., Smith, C. L., Presley, J. F., Worman, H. J., and Lippincott-Schwartz, J. (1997) *J. Cell Biol.* **138,** 1193–1206
22. Lin, R., Murtazina, R., Cha, B., Chakraborty, M., Sarker, R., Chen, T. E., Lin, Z., Hogema, B. M., de Jonge, H. R., Seidler, U., Turner, J. R., Li, X., Kovbasnjuk, O., and Donowitz, M. (2011) *Gastroenterology* **140,** 560–571
23. Rizzo, M. A., Springer, G., Segawa, K., Zipfel, W. R., and Piston, D. W. (2006) *Microsc. Microanal.* **12,** 238–254
24. Donowitz, M., Cohen, M. E., Gould, M., and Sharp, G. W. (1989) *J. Clin. Invest.* **83,** 1953–1962
25. Li, X., Zhang, H., Cheong, A., Leu, S., Chen, Y., Elowsky, C. G., and Donowitz, M. (2004) *J. Physiol.* **556,** 791–804
26. Sarker, R., Valkhoff, V. E., Zachos, N. C., Lin, R., Cha, B., Chen, T. E., Guggino, S., Zizak, M., de Jonge, H., Hogema, B., and Donowitz, M. (2011) *Am. J. Physiol. Cell Physiol.* **300,** C771–C782
27. Gill, R. K., Saksena, S., Tyagi, S., Alrefai, W. A., Malakooti, J., Sarwar, Z., Turner, J. R., Ramaswamy, K., and Dudeja, P. K. (2005) *Gastroenterology* **128,** 962–974
28. Musch, M. W., Arvans, D. L., Walsh-Reitz, M. M., Uchiyama, K., Fukudo, M., and Chang, E. B. (2007) *Am. J. Physiol. Gastrointest. Liver Physiol.* **292** G1549–G1558
29. Musch, M. W., Arvans, D. L., Wang, Y., Nakagawa, Y., Solomaha, E., and Chang, E. B. (2010) *Am. J. Physiol. Gastrointest. Liver Physiol.* **298,** G203–G211
30. Hayashi, H., Szászi, K., Coady-Osberg, N., Furuya, W., Bretscher, A. P., Orlowski, J., and Grinstein, S. (2004) *J. Gen. Physiol.* **123,** 491–504
31. Pang, Z. P., and Südhof, T. C. (2010) *Curr. Opin. Cell Biol.* **22,** 496–505
32. Murtazina, R., Kovbasnjuk, O., Chen, T. E., Zachos, N. C., Chen, Y., Kocinsky, H., Hogema, B. M., Seidler, U. E., de Jonge, H. R., and Donowitz, M. (2011) *Am. J. Physiol. Cell Physiol.* **301,** C126–C136
33. Choi, J. W., Lee-Kwon, W., Jeon, E. S., Kang, Y. J., Kawano, K., Kim, H. S., Suh, P. G., Donowitz, M., and Kim, J. H. (2004) *Biochim. Biophys. Acta* **1683,** 59–68
34. Banday, A. A., and Lokhandwala, M. F. (2011) *Am. J. Physiol. Renal Physiol.* **301,** F364–F370
35. Zachos, N. C., Hodson, C., Kovbasnjuk, O., Li, X., Thelin, W. R., Cha, B., Milgram, S., and Donowitz, M. (2008) *Cell. Physiol. Biochem.* **22,** 693–704
36. Akhter, S., Kovbasnjuk, O., Li, X., Cavet, M., Noel, J., Arpin, M., Hubbard, A. L., and Donowitz, M. (2002) *Am. J. Physiol. Cell Physiol* **283,** C927–C940
37. Alexander, R. T., Furuya, W., Szászi, K., Orlowski, J., and Grinstein, S. (2005) *Proc. Natl. Acad. Sci. U.S.A.* **102,** 12253–12258
38. Alexander, R. T., and Grinstein, S. (2009) *J. Exp. Biol.* **212,** 1630–1637
39. Li, X., Galli, T., Leu, S., Wade, J. B., Weinman, E. J., Leung, G., Cheong, A., Louvard, D., and Donowitz, M. (2001) *J. Physiol.* **537,** 537–552
40. Murtazina, R., Kovbasnjuk, O., Donowitz, M., and Li, X. (2006) *J. Biol. Chem.* **281,** 17845–17855
41. Riquier, A. D., Lee, D. H., and McDonough, A. A. (2009) *Am. J. Physiol. Cell Physiol.* **296,** C900–C910
42. Biemesderfer, D., DeGray, B., and Aronson, P. S. (2001) *J. Biol. Chem.* **276,** 10161–10167
43. Lin, S., Yeruva, S., He, P., Singh, A. K., Zhang, H., Chen, M., Lamprecht, G., de Jonge, H. R., Tse, M., Donowitz, M., Hogema, B. M., Chun, J., Seidler, U., and Yun, C. C. (2010) *Gastroenterology* **138,** 649–658
44. McDonough, A. A., and Biemesderfer, D. (2003) *Curr. Opin. Nephrol. Hypertens.* **12,** 533–541
45. Yang, L. E., Maunsbach, A. B., Leong, P. K., and McDonough, A. A. (2005) *J. Am. Soc. Nephrol.* **16,** 2890–2896